Displacement Reconstructions in Ultrasound Elastography

Guillaume Bal, Sébastien Imperiale

Displacement reconstructions in ultrasound elastography

Guillaume Bal * Sébastien Imperiale †

March 9, 2015

Abstract

We consider the reconstruction of internal elastic displacements from ultrasound measurements, which finds applications in the medical imaging modality called elastography. By appropriate interferometry and windowed Fourier transforms of the ultrasound measurements, we propose a reconstruction procedure of the vectorial structure of spatially varying elastic displacements in biological tissues. This provides a modeling and generalization of scalar reconstruction procedures routinely used in elastography. The proposed algorithm is justified using a single scattering approximation and local asymptotic analysis. Its validity is assessed by numerical simulations.

1 Introduction

Elastography has established itself as an important imaging modality to quantify the elastic properties of biological tissues [8, 9, 16, 18, 19, 20, 21]. In most settings of elastography, the first step in the modality is the reconstruction of internal elastic displacements or strain tensors. This paper is concerned with Ultrasound Elastography, which includes Strain Elastography [18, 19] and Transient Elastography (or Shear-wave Elastography) [8, 9], and aims to reconstruct the elastic displacements from ultrasonic echoes. Internal displacements may also be obtained by another method, not considered in this paper, which combines elastic displacements with magnetic resonance imaging; see [14, 15, 16, 17, 21] for additional information on Magnetic Resonance Elastography.

Ultrasound Elastography leverages a physical coupling between elastic displacements and scattering of ultrasound. Elastic (shear) waves propagate relatively slowly through biological tissues (on the order of m/s). They generate displacements of cells, which may be seen as weak scatterers for the much faster (on the order of 1500 m/s) probing ultrasonic (compressional) waves. Ultrasonic probing pulses emitted a few (or fractions of a) ms apart encounter a slightly modified environment, which provides information about the elastic displacements.

The main objective of this paper is a modeling of the interaction of the probing ultrasound with the underlying tissues perturbed by elastic displacements. There is an important literature on this

*Department of Applied Physics and Applied Mathematics, Columbia University, New York NY, 10027; gb2030@columbia.edu

†INRIA, Saclay Ile-de-France, 91120 Palaiseau, France

subject, mostly modeling ultrasound measurements as time traces on a given ultrasonic transducer and estimating time delays; see for instance [19, 23, 9] and their references. In this paper, we propose a model that allows us to reconstruct the vectorial structure of the elastic displacements. It is well-known that displacements generate phase shifts in the Fourier domain, which may be detected by appropriate interferometric techniques. Interferometry of time traces allows one to garner precise information about displacements in a spatially one-dimensional setting. We propose here reconstructions based on space-time interferometry (or more precisely space-time windowed Fourier transforms) that provide a full characterization of the elastic displacements.

Ultrasound are modeled as acoustic waves propagating in a disordered environment. Their modeling is therefore a problem of wave propagation in highly heterogeneous media [10, 22]. More precisely, we aim to understand the correlation (interferometry) of two ultrasonic field propagating in slightly different media. This was analyzed in the context of time reversed waves in random media in, e.g., [1, 6]. The method in the latter reference may be used to derive the reconstruction procedure for the elastic displacements proposed below. However, such a method requires more restrictive spatial and temporal averaging to obtain statistically stable reconstructions. We therefore present in section 3 below a more direct modeling of the ultrasound propagation in the heterogeneous environment based upon single scattering approximation.

The reconstructed internal elastic displacements do not provide quantitative properties of the biological tissues. A second inverse problem, often referred to as a hybrid inverse problem, needs to be solved. We do not consider this step here and refer the reader to, e.g., [2, 3, 12] for more information on hybrid inverse problems and to [4, 5, 7] for quantitative reconstructions of elastic properties using scalar and vectorial elasticity models.

The rest of the paper is structured as follows. Section 2 presents the main results of this paper and the reconstruction of vectorial spatially varying elastic displacements from appropriate windowed Fourier transforms of spatio-temporal ultrasound measurements. The derivation of the reconstruction and its main properties using models of wave propagation in heterogeneous media is given in section 3. Finally, numerical reconstructions of displacements are displayed in section 4. Some concluding remarks and perspective are given in section 5.

2 Reconstruction procedure

This section presents the main results of the paper as well as the principal hypotheses on the underlying biological medium. We refer to section 3 on the derivation of the main results for additional details.

Throughout this paper, the elastic displacement is denoted by $\tau(x)$ for $x \in X \subset \mathbb{R}^n$ with typically $n = 3$. Here X is the spatial domain in which we wish to reconstruct the displacement. We do not consider the generation of the displacement itself. It could be done by compression, by acoustic radiation force, or by any other means; see [21] for a review. We assume that the elastic waves that generate such a displacement propagate at a much lower speed than the ultrasonic waves used to probe it so that the displacement $\tau(x)$ is approximately independent of time during the ultrasound probing. In a static compression, $\tau(x)$ would be the displacement between a body at rest and the body experiencing a small displacement; in a dynamic setting such as transient elastography, $\tau(x)$ would be the (even smaller) displacement between two probing frames.

We denote by $u(t,x)$ and $u_\tau(t,x)$ the propagating acoustic fields (ultrasound) in the absence and the presence of the displacement. An acoustic pulsed source is emitted in the vicinity of a point z_0 and close to time $t=0$; see section 3 for a more precise description of the source, whose details do not matter for the reconstruction. We consider space-time measurements in the vicinity of the point (t_0,x_0).

The main assumption on the propagation of ultrasound is that the underlying medium (biological tissues) is highly heterogeneous but weakly scattering. For concreteness, we also assume that the macroscopic sound speed is constant and equal to c (typically that of water). In such a setting, we may assume that $u(t,x)$ is well approximated by a single scattering approximation. Heuristically, the acoustic signal emitted at (in the vicinity of) $(0,z_0)$ thus propagates along straight lines until it scatters at times $s>0$ at a point y_0 such that $|y_0-z_0|=c\,s$. Signals are then measured at (in the vicinity of) (t_0,x_0) provided that $c\,t_0=|x_0-y_0|+|y_0-z_0|$. We observe that the points y_0 satisfying such constraints live on an ellipsoid. The point y_0, where scattering occurred and which will provide information about $\tau(y_0)$, is therefore not uniquely determined. What we need is to obtain directional information about the measured signal $u(t,x)$. This is where windowed Fourier transforms (also known mathematically as Fourier-Bros-Iagolnitzer (FBI) transforms) provide the required information. Let us define for a wavenumber $k\in\mathbb{R}^n$

$$v(t_0,x_0,k)=\int_{\mathbb{R}^n} e^{-\frac{\alpha}{2}|x-x_0|^2}e^{-ik\cdot(x-x_0)}u(t_0,x)dx. \tag{1}$$

This windowed Fourier transform (FBI transform) constrains the signal in the $\alpha^{-\frac{1}{2}}$ vicinity of x_0 and takes is Fourier transform for the wavenumber k. The choice of $|k|$ is made by the choice of the probing ultrasound: $c\,|k|$ is a frequency (for instance the carrier frequency) that is present in the pulsed ultrasound generated at z_0. If L is the diameter of the spatial domain X, we assume that $|k|L\gg 1$ to obtain a good resolution. We want $\alpha^{\frac{1}{2}}L\gg 1$ to obtain localization in the vicinity of x_0 and $\alpha^{\frac{1}{2}}\ll|k|$ in order to obtain good directional information in the direction $\hat{k}=k/|k|$. An optimal choice is $\alpha\sim|k|L^{-1}$. The processed signal v then provides a $(L|k|)^{-\frac{1}{2}}$ localization both in the physical and wavenumber spaces, which is optimal by the Heisenberg principle.

The above transform requires measurement of $u(t_0,x)$ in the spatial vicinity of x_0 at a given time t_0. In practice, it is more convenient to consider an array of ultrasonic transducers that capture time traces of the acoustic signal. Let us decompose $x=x_0+x_1e_1+x'$ with e_1 the direction orthogonal to the transducer array and x' the coordinates along the array. We then decompose $k=k_1e_1+k'$ with $k_1<0$ and k' orthogonal to e_1 and define the space-time FBI transform

$$w(t_0,x_0,k)=\int_{\mathbb{R}^n} e^{-\frac{\alpha}{2}(c^2(t-t_0)^2+|x'|^2)}e^{-i(c|k|(t-t_0)+k'\cdot x')}u(t,0,x')dx'dt. \tag{2}$$

In the above phase $c|k|(t-t_0)+k'\cdot x'$, we recognize the dispersion relation $\omega=c|k|$ with the choice of sign obtained from knowing that the signal propagates in the direction of negatives values of x_1. We assume that the displacement $\tau(x)$ is supported in the half space $x_1>0$; i.e., $X\subset\{x\in\mathbb{R}^n;x_1>0\}$.

In both (1) and (2), the domain of integration is $\mathbb{R}^n$ and $\mathbb{R}^{n-1}\times\mathbb{R}$. Note that the Gaussian term decays rapidly as $|x-x_0|$ or $c^2(t-t_0)^2+|x'|^2$ increases. In practice, the infinite domains of integration are replaced by finite domains with the assumption that the detector array is large enough so that most of the signal in (1) and (2) is captured.

Above, u, v, and w are acoustic signals for the (unknown) underlying biological tissues in a reference configuration. We assume that at a later time frame, the biological tissue has undergone a (vectorial) displacement given by $\tau(x)$. The corresponding probing acoustic signals are then denoted by u_τ, v_τ, and w_τ, respectively. In the setting of a planar array of ultrasonic transducers, we therefore have access to w and w_τ. Qualitative transient elastography concerns the reconstruction of $\tau(x)$ from such information.

The source location $(0, z_0)$ and measurement location (t_0, x_0, k) are fixed in our analysis. We assume that $c\,t_0 > |x_0 - z_0|$ so that the measurements would vanish in the absence of heterogeneities in the underlying medium. In the single scattering setting, scattering has to occur at the uniquely determined point $y_0 = y_0(t_0, x_0, k)$ such that (see also Figure 1)

$$\hat{k} = \frac{k}{|k|} = \frac{x_0 - y_0}{|x_0 - y_0|} \quad \text{and} \quad c\,t_0 = |x_0 - y_0| + |y_0 - z_0|. \tag{3}$$

We then define the vectors, which are functions of (t_0, x_0, k, z_0):

$$\hat{\psi} = \frac{y_0 - z_0}{|y_0 - z_0|}, \qquad \phi = \hat{k} - \hat{\psi}. \tag{4}$$

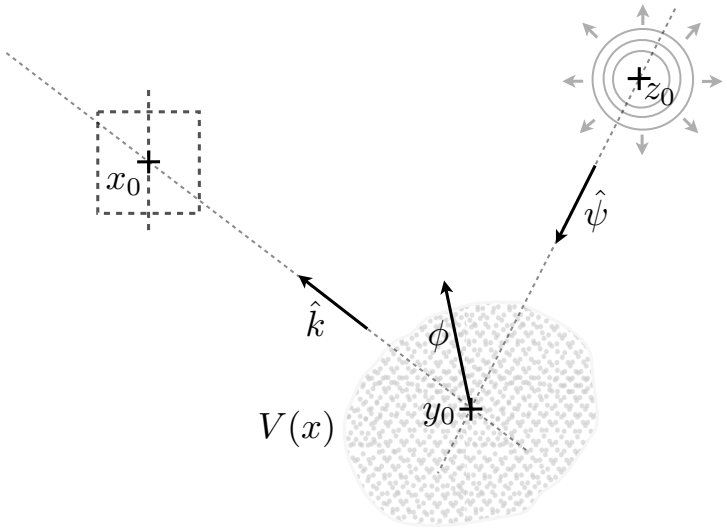

Figure 1: Schematic of the configuration: The initial condition is located around z_0, the measurement region is located around x_0 (the dotted square for the computation of v or the dotted line for the computation of w), the displacement is reconstructed at y_0, the heterogeneities (i.e. the scatterers) are given by the function $V(x)$.

We are now ready to present the reconstruction of the displacement $\tau(y)$:

Reconstruction Procedure. The main result of this paper is that, under appropriate assumptions detailed later:

$$\frac{w_\tau(t_0, x_0, k)}{w(t_0, x_0, k)} \approx \frac{v_\tau(t_0, x_0, k)}{v(t_0, x_0, k)} \approx e^{i|k|\tau(y_0)\cdot\phi}\Big(1 \;+\; O\Big(\Big(\frac{1}{L\sqrt{\alpha}} + \frac{\sqrt{\alpha}}{|k|}\Big)\big(1 + |\nabla\tau(y_0)|\big)\Big)\Big). \tag{5}$$

In other words, the measured ratios $\frac{w_\tau(t_0,x_0,k)}{w(t_0,x_0,k)}$ or $\frac{v_\tau(t_0,x_0,k)}{v(t_0,x_0,k)}$ are unit complex numbers whose arguments divided by $|k|$ equal $\tau(y_0)\cdot\phi$ with $\phi=\phi(t_0,x_0,k,z_0)$ defined in (4). More specifically, writing for instance $\frac{w_\tau(t_0,x_0,k)}{w(t_0,x_0,k)}$, we observe, provided that $|k||\tau|$ is sufficiently small, that

$$\tau(y_0)\cdot\phi \approx \frac{1}{|k|}\arg\left(\frac{w_\tau(t_0,x_0,k)}{w(t_0,x_0,k)}\right).$$

As mentionned in the introduction, practical ultrasound elastography methodologies are based on 1D cross-correlation algorithms (see [9] for an overview and detailed references). In these algorithms, the vectorial structure of the displacement is not taken into account. This bias is minimized in experiments by generating a displacement polarized in the *axial* direction, i.e., (x_0,y_0,z_0) are aligned; this is the principle of the $1D$-Transient elastography. The justification of formula (5) given below sets some theoretical background for a development in the direction of fully vectorial reconstructions of the elastic displacement.

We make several remarks regarding the reconstruction:

Signal. The above formula takes the ratio of two fields, which better be non-vanishing. As will become more apparent in the next section, w_τ and w are well approximated by the product of two quantities: (i) the frequency content of the acoustic pulse at the wavenumber $|k|\hat{\psi}$, and (ii) the amount of scattering generated at y_0 for the wavenumber $|k|\phi$ (see (13) below). Since scattering increases rapidly with $|k|$ (as the fourth power of $|k|$ for Rayleigh scattering), we need to choose k in the acoustic pulse so that scattering is strong enough to be detected in w and weak enough so that multiple scattering can be neglected. This is a good approximation for the standard applications of ultrasound in the $1-10$MHz range.

Statistical Stability. Both w_τ and w are random fields in the sense that they depend on the unknown (small scale) scattering properties of the underlying biological tissues. However, the ratio in (5) is approximately statistically stable (i.e., independent of the specific realization of the scattering) and nothing prevents the denominator to be close to 0, which creates some numerical instabilities. The statistical stability may heuristically be improved by considering the following averaging procedure (written for (w,w_τ) for concreteness)

$$e^{i|k|\tau(y_0)\cdot\phi} \approx \frac{\int (w_\tau w^*)(t_0+t,x_0+x,k+q)d\nu(t,x,q)}{\int |w|^2(t_0+t,x_0+x,k+q)d\nu(t,x,q)}, \tag{6}$$

with ν a continuous or discrete measure supported in a sufficiently small vicinity of $(0,0,0)$ so that $\tau(y(t_0+t,x_0+x,k+q))$ is close to $\tau(y_0)$ for all (t,x,q) in the support of ν. The interferometric measurement $w_\tau w^*$ may be seen as the correlation of the perturbed field w_τ with the unperturbed field w. Note also that the denominator in (6) is non-vanishing for measures ν with sufficiently broad support; see also our numerical simulations in section 4.

Resolution. The formula (5) hinges on $\tau(y)$ varying more slowly than the other quantities involved, typically the wavelength of the probing pulse and the correlation length of the scattering

medium. As we shall see, (5) holds with an error that is proportional to $\left(\frac{1}{\sqrt{\alpha}} + \frac{L\sqrt{\alpha}}{|k|}\right)|\nabla\tau(y_0)|$. Choosing α optimally as $|k|/L$, we observe that variations of τ at (and faster than) the spatial scale $\alpha^{-\frac{1}{2}} = L^{\frac{1}{2}}/|k|^{\frac{1}{2}}$ cannot be reconstructed accurately. The procedure still has the potential to reconstruct sub-millimetric variations in $\tau(y_0)$ with the use of $5-10$MHz ultrasonic pulses. This inherent limitation of the method is confirmed by our numerical simulations and those in [13]

Aliasing. The above algorithm provides a means to reconstruct $\tau(y_0)\cdot\phi$ with $\phi = \phi(t_0, x_0, k)$ given in (4) from evaluating the argument in (5) and dividing by $|k|$. This reconstruction is unambiguous provided that $|k||\tau||\phi| < \pi$, which holds when $2|k||\tau| < \pi$. In practice, displacements are quite small and the latter constraint is satisfied. When this is not the case, the aliasing issue can be remedied by choosing smaller frequencies $|k|$ or multiple frequencies k; see [13].

Echo Mode. When the source and the detector are located at the same point with $x_0 = z_0$ then $\hat{\psi} = -\hat{k}$ and $\phi = 2\hat{k}$. If the array is moreover orthogonal to $\hat{k}$ so that $k' = 0$ in (2), then (5) provides the displacement $\tau(y_0)\cdot\hat{k}$ along the line $y_0 = x_0 - s\hat{k}$ by considering a windowed Fourier transform in time for the average ultrasound measured on the ultrasonic array.

Vectorial reconstruction. The above procedure can be repeated by changing the location of the source z_0 and the array (t, x_0, k) parameters. For a fixed (z_0, x_0), the whole domain y_0 may be swept by changing t and the direction $\hat{k}$. This allows us to reconstruct $\tau(y)\cdot\phi(t, k; x_0)$ in a direction ϕ dictated by the geometry. We then verify that the full vectorial structure of $\tau(y)$ may be reconstructed by choosing n source locations z_n that do not lie on a subspace of co-dimension greater than 2. In dimension $n = 3$, this means choosing three different source locations z_1, z_2, and z_3 that do not lie on the same line. For instance, with $x_0 = 0$ and an orientation of the array given by e_1, we could choose $z_1 = x_0 = 0$, $z_2 = (0, d, 0)$ and $z_3 = (0, 0, d)$ for any $d \neq 0$. This issue is considered in more detail in section 4.

Triangulation. This paper considers the setting of a localized source in the vicinity of z_0 with a wide radiation pattern. Measurements at (t_0, x_0) then correspond to single scattering occurring at points y such that $c\,t_0 = |x_0 - y| + |y - z_0|$, which do not uniquely characterize y. The role of the FBI transform is to further localize the measurements in space and direction to uniquely determine a point y_0 that satisfies the above constraint and lives on the line $x_0 - s\hat{k}$ for some $s > 0$. Other triangulation procedures could also be considered, for instance using a source at z_0 that only radiates in a specific direction. We then verify that measurements of $u(t_0, x_0)$ also provide information about $\tau(y_0)\cdot\phi$ at an appropriate uniquely defined y_0; see also [13].

3 Derivation of the reconstruction procedure

We first model the propagation of the acoustic signal in the underlying medium, typically biological tissues in applications of elastography. We recall that the elastic shear waves and ultrasound (compressional) waves propagate at significantly different speeds and may be considered with a reasonable accuracy as decoupled. Ultrasound are modeled here as propagating in an isotropic acoustic medium

with sound speed $c(x)$ that we recast as

$$\frac{1}{c^2(x)} = \frac{1}{c^2}(1 - V(x)),$$

with V a spatially varying index of refraction and c a constant macroscopic sound speed (e.g., that of water). We assume that V is a realization of a statistically homogeneous random distribution around a region of interest. By rescaling time $L^{-1}c\,t \to t$ and space $L^{-1}x \to x$ (and $V(L^{-1}x) \to V(x)$) we may assume that $c = L = 1$. The model for the acoustic signal is then the following wave equation

$$(\partial_t^2 - \Delta)u = V\partial_t^2 u. \tag{7}$$

This is augmented with initial conditions at $t = 0$ given by

$$u(0, x) = 0, \qquad \partial_t u(0, x) = f(x - z_0). \tag{8}$$

The initial condition f could be generated by a time pulse emitted at z_0 for small negative times whose emitted signal is evaluated at $t = 0$; see also section 4. The pressure $u(0, x)$ would then not necessarily vanish. More general initial conditions than (8) can easily be accounted for at the expense of slightly more cumbersome notation and so we restrict ourselves to (8) for simplicity.

Single scattering approximation. Let us introduce

$$(\partial_t^2 - \Delta)u_0 = 0, \qquad (\partial_t^2 - \Delta)u_1 = V\partial_t^2 u_0,$$

with $\partial_t u_0(0, x) = f(x)$ and all other initial conditions for u_0 and u_1 vanishing. Then for $v = u - u_0 - u_1$ we have

$$(\frac{1}{c^2(x)}\partial_t^2 - \Delta)v = V\partial_t^2 u_1.$$

Considering the energy norm

$$E_c[v](t) = \int_{\mathbb{R}^n} \big(\partial_t v)^2 + c^2(x)|\nabla v|^2\big)dx,$$

it is standard that

$$E_c[v]^{\frac{1}{2}}(t) \le C\,\|V\|_\infty \int_0^t \left(\int_{\mathbb{R}^n} (\partial_t^2 u_1)^2 dx\right)^{\frac{1}{2}} ds \le C\,\|V\|_\infty \int_0^t E_c[\partial_t u_1]^{\frac{1}{2}}(s)\; ds,$$

with C a generic constant depending only on the bounds for$c(x)$. This energy identity implies

$$E_c[v]^{\frac{1}{2}}(t) \le C\,\|V\|_\infty^2 \int_0^t \int_0^s E_c[\partial_t^3 u_0]^{\frac{1}{2}}(r)\; dr\; ds.$$

Assuming that u_0 has sufficiently small time derivatives compared to V we find that u_1 has energy of order V while v has energy of order $V^2 \ll V$, which is now neglected. At the detector level, only u_1, which we now relabel as u, is measured since the ballistic part u_0 vanishes on the support of the detector for times t (at least slightly) larger than $|x_0 - z_0|$.

Model of propagation. Within the single scattering approximation, we thus have u modeled by

$$(\partial_t^2 - \Delta)u = V\partial_t^2 u_0 = V\Delta u_0.$$

Note that Δu_0 solves the wave equation with initial conditions given by $(\Delta u_0)(0,x) = 0$ and $\partial_t(\Delta u_0)(0,x) = (\Delta f)(x)$ so that it is really Δf and not f that is propagated in our model.

Define now the Green's function as the solution to

$$(\partial_t^2 - \Delta)G = \delta(t)\delta(x)$$

which is given in dimension $n = 3$ by

$$G(t,x) = \frac{1}{4\pi|x|}\delta(t - |x|).$$

Thus, we may write u in dimension $n = 3$ as

$$\begin{aligned}(4\pi)^2 u(t,x) &= \int_0^t \int_{\mathbb{R}^6} 4\pi G(s, x-y)V(y)4\pi G(t-s, y-z)(\Delta f)(z)dsdydz \\ &= \int_{\mathbb{R}^6} \frac{\delta(t - |x-y| - |y-z|)}{|x-y||y-z|}V(y)(\Delta f)(z)dydz. \end{aligned} \tag{9}$$

To avoid unnecessary technical difficulties, we assume that $V(y)$ vanishes in the vicinity of the support of Δf and the detector array so that $|x-y||y-z|$ is uniformly bounded from below on the support of V by a positive constant.

The formula (5) is obtained asymptotically in the limit of large frequencies of probing. We thus introduce a small parameter $0 < \varepsilon \ll 1$ and consider initial conditions of frequency $|k|/\varepsilon$ with $|k|$ a rescaled wavenumber. The probing pulse has frequencies of order ε^{-1} and is emitted in the vicinity of z_0. We thus replace the initial condition $(\Delta f)(x)$ by $(\Delta f)(\frac{z-z_0}{\varepsilon})$. Such an initial condition could be renormalized by a multiplicative factor $\varepsilon^{-\frac{3}{2}}$ to preserve its L^2 norm. However, since u is linear both in (Δf) and in V, we do not keep track of such renormalizations.

Scaling. As waves with frequency of order $|k|/\varepsilon$ propagate in the heterogeneous medium modeled by V, they primarily interact with features of V of similar frequency $|k|/\varepsilon$ (see, e.g., [1, 22]). We therefore assume that the correlation length of V is of order ε and set

$$V \equiv V_{y_0}(\frac{y - y_0}{\varepsilon}).$$

Since the frequencies of the measured signals v and w are now of order ε^{-1}, for the rest of the paper, we introduce rescaled versions of (1) and (2). We only consider the case of v to simplify and thus introduce (neglecting the constant $(4\pi)^2$ that cancels out when ratios are taken in formula (5))

$$v_\varepsilon(t_0, x_0, k) = \int e^{-\frac{\alpha}{2\varepsilon}(x-x_0)^2} e^{-i\frac{k}{\varepsilon}\cdot(x-x_0)} \frac{\delta(t_0 - |x-y| - |y-z|)}{|x-y||y-z|} V_{y_0}(\frac{y-y_0}{\varepsilon})(\Delta f)(\frac{z-z_0}{\varepsilon})dxdydz. \tag{10}$$

In the above expression, we have also rescaled $\alpha \to \frac{1}{\varepsilon}\alpha$ as the appropriate spatial concentration scale about the point x_0.

Let us now model the elastic displacement. Since frequency is of the form $|k|/\varepsilon$ and frequency times displacement has to be sufficiently small to avoid aliasing, we rescale the elastic displacement as $\varepsilon\tau(y)$. Each point y inside the domain of interest is therefore shifted to $y+\varepsilon\tau(y)$. As a consequence, we obtain the rescaled shifted signal

$$v_{\varepsilon\tau}(t_0,x_0,k)=\int e^{-\frac{\alpha}{2\varepsilon}(x-x_0)^2}e^{-i\frac{k}{\varepsilon}\cdot(x-x_0)}\frac{\delta(t_0-|x-y|-|y-z|)}{|x-y||y-z|}V_{y_0}\Big(\frac{y-y_0}{\varepsilon}+\tau(y)\Big)(\Delta f)(\frac{z-z_0}{\varepsilon})dxdydz. \tag{11}$$

The objective of the rest of this section is to obtain a macroscopic model for $\frac{v_{\varepsilon\tau}}{v_\varepsilon}$. The reader can verify that the same reasoning provides a macroscopic model for $\frac{w_{\varepsilon\tau}}{w_\varepsilon}$.

Asymptotic expansion. We now justify formula (5) in the case where all the scattering occurs in a ε-vicinity of y_0. More precisely it consists to assume that

$$\text{supp}\left(V_{y_0}(\frac{y-y_0}{\varepsilon})\right) \quad \text{and} \quad \text{supp}\left(\Delta f(\frac{z-z_0}{\varepsilon})\right)$$

are included in (two disjoints) balls with ε-independent radius. Note that since V_{y_0} is also bounded by assumption, it is then integrable.

We recall that y_0 is uniquely defined by the constraints $t_0=|x_0-y_0|+|y_0-z_0|$ and $\hat{k}=\widehat{x_0-y_0}$ and that $\hat{\psi}=\widehat{y_0-z_0}$ and $\phi=\hat{k}-\hat{\psi}$, which is not a unit vector in general. We now change variables as follows. We rewrite

$$y\to y_0+\varepsilon y, \qquad z\to z_0+\varepsilon z, \qquad x\to x_0+\varepsilon x_1\hat{k}+x'\varepsilon^{\frac{1}{2}},$$

with x' orthogonal to $\hat{k}$. Up to multiplication by $\varepsilon^{(5\times3+1)/2}$ we have to analyze

$$\int e^{-\frac{\alpha}{2}(|x'|^2+\varepsilon x_1^2)}e^{-i|k|x_1}\frac{\delta(t-|x_0-y_0+x'\varepsilon^{\frac{1}{2}}+\varepsilon(x_1\hat{k}-y)|-|y_0-z_0+\varepsilon(y-z)|)}{|x_0-y_0+x'\varepsilon^{\frac{1}{2}}+\varepsilon(x_1\hat{k}-y)||y_0-z_0+\varepsilon(y-z)|}V_{y_0}(y)(\Delta f)(z)dxdydz.$$

In the presence of a displacement, $V_{y_0}(y)$ above is replaced by $V_{y_0}(y+\tau(y_0+\varepsilon y))$. We wish to use the delta function to integrate out the x_1 variable. This is done by using the following Taylor expansions

$$|x+\delta x|=|x|+\delta x\cdot\hat{x}+\frac{1}{2|x|}(|\delta x|^2-(\delta x\cdot\hat{x})^2)+O(\delta x^3).$$

We then find that $t-|x_0-y_0+x'\varepsilon^{\frac{1}{2}}+\varepsilon(x_1\hat{k}-y)|-|y_0-z_0+\varepsilon(y-z)|$ takes the form

$$\varepsilon(x_1-\phi\cdot y-\hat{\psi}\cdot z+\frac{|x'|^2}{2\,|x_0-y_0|})+\varepsilon^{\frac{3}{2}}\varphi_1(x_1,x',y,z)$$

for φ_1 a bounded function for the original (x,y,z) sufficiently close to (x_0,y_0,z_0). We can then change the variable $x_1+\varepsilon^{\frac{1}{2}}\varphi_1(x_1,x',y,z)\to x_1$ to finally obtain an expression for x_1

$$\varepsilon(x_1-\phi\cdot y-\hat{\psi}\cdot z+\frac{|x'|^2}{2\,|x_0-y_0|})+\varepsilon^{\frac{3}{2}}\varphi_2(x',y,z)=0.$$

After replacing the x_1 variable and integration in the x' variable we further obtain the expression (again up to a multiplicative constant depending on $|k|$)

$$\int e^{-i|k|(y\cdot\phi+z\cdot\hat{\psi})}V_{y_0}(y)(\Delta f)(z)\frac{(1+\varepsilon^{\frac{1}{2}}\varphi_\varepsilon(y,z)))}{|x_0-y_0||y_0-z_0|}dydz \equiv I_\varepsilon(t_0,x_0,k).$$

Here $\varphi_\varepsilon(y,z)$ is uniformly bounded in y and z over the (bounded) domains of integration and $\varepsilon^{\frac{1}{2}}\varphi_\varepsilon(y,z)=o(1)$. In the presence of a displacement, we have

$$\int e^{-i|k|(y\cdot\phi+z\cdot\hat{\psi})}V_{y_0}(y+\tau(y_0+\varepsilon y))(\Delta f)(z)\frac{(1+\varepsilon^{\frac{1}{2}}\varphi_\varepsilon(y,z))}{|x_0-y_0||y_0-z_0|}dydz \equiv I_{\varepsilon\tau}(t_0,x_0,k).$$

Note that $v_{\varepsilon\tau}/v_\varepsilon = I_{\varepsilon\tau}/I_\varepsilon$. We now change variables

$$\mathfrak{y} = y+\tau(y_0+\varepsilon y) \text{ so that } y=\mathfrak{y}-\tau(y_0)+O(\varepsilon|\nabla\tau|) \tag{12}$$

This allows us to recast the above expression as

$$I_{\varepsilon\tau} = e^{i|k|\tau(y_0)\cdot\phi}\int e^{-i|k|(y\cdot\phi+z\cdot\hat{\psi})}V_{y_0}(y)(\Delta f)(z)\frac{(1+\varepsilon^{\frac{1}{2}}\varphi_\varepsilon(y,z)+O(\varepsilon|\nabla\tau|))}{|x_0-y_0||y_0-z_0|}dydz.$$

This shows that

$$\frac{v_{\varepsilon\tau}}{v_\varepsilon} = e^{i|k|\tau(y_0)\cdot\phi}\frac{\int e^{-i|k|(y\cdot\phi+z\cdot\hat{\psi})}V_{y_0}(y)(\Delta f)(z)(1+\varepsilon^{\frac{1}{2}}\varphi_\varepsilon(y,z)+O(\varepsilon|\nabla\tau|))dydz}{\int e^{-i|k|(y\cdot\phi+z\cdot\hat{\psi})}V_{y_0}(y)(\Delta f)(z)(1+\varepsilon^{\frac{1}{2}}\varphi_\varepsilon(y,z))dydz} \approx e^{i|k|\tau(y_0)\cdot\phi}$$

by neglecting the terms $\varepsilon^{\frac{1}{2}}\varphi_\varepsilon(y,z)$ and $O(\varepsilon|\nabla\tau|)$). This is (5). When V_{y_0} and (Δf) are L^1 functions uniformly in ε and $\tau(y)$ is independent of ε, then as $\varepsilon\to 0$ the above integrals converge to the same constant

$$\hat{V}_{y_0}(|k|\phi)\widehat{(\Delta f)}(|k|\hat{\psi}). \tag{13}$$

Provided that the latter does not vanish, then the ratio of measurements is approximately given by $e^{i|k|\tau(y_0)\cdot\phi}$ as an application of the Lebesgue dominated convergence theorem. Note that the ratio of the measurements is therefore approximately deterministic even though both measurements are random.

Then (6) follows provided μ is supported on a domain such that $y=y(t,x,q)$ remains sufficiently close to y_0 (such that $\tau(y)$ remains close to $\tau(y_0)$).

Statistical Stability of the ratio and resolution. In the range $\varepsilon^{\frac{1}{2}}\varphi_\varepsilon \ll \varepsilon|\nabla\tau|$, we can estimate the statistical stability of the measurements. Up to lower-order terms, we have that

$$\mathfrak{y} \approx y+\tau(y_0)+\varepsilon y\cdot\nabla\tau = \tau(y_0)+(I+(\varepsilon\nabla\tau(y_0))^t)y \quad \text{ so that } \quad y\approx (I+(\varepsilon\nabla\tau(y_0))^t)^{-1}(\mathfrak{y}-\tau(y_0))$$

Therefore, we find that $I_{\varepsilon\tau}$ is approximately given by

$$I_{\varepsilon\tau} \approx e^{i|k|(I+(\varepsilon\nabla\tau(y_0))^t)^{-1}\tau(y_0)\cdot\phi}\frac{\widehat{(\Delta f)}(|k|\hat{\psi})}{|x_0-y_0||y_0-z_0|}\frac{\hat{V}_{y_0}(|k|(I+\varepsilon\nabla\tau(y_0))^{-1}\phi)}{\det(I+\varepsilon\nabla\tau(y_0))}.$$

The ratio $\frac{v_{\varepsilon\tau}}{v_\varepsilon}$ is therefore approximately given by

$$\frac{v_{\varepsilon\tau}}{v_\varepsilon} \approx \frac{e^{i|k|(I+(\varepsilon\nabla\tau(y_0))^t)^{-1}\tau(y_0)\cdot\phi}}{\det(I+\varepsilon\nabla\tau(y_0))} \frac{\hat{V}_{y_0}(|k|(I+\varepsilon\nabla\tau(y_0))^{-1}\phi)}{\hat{V}_{y_0}(|k|\phi)}. \tag{14}$$

This is a random variable whose variance can be estimated for a model of randomness of V. When $\varepsilon|\nabla\tau|$ is large, then $\hat{V}$ is estimated at a different wavenumber and the variance is expected to be large. When $\hat{V}$ is a smooth function, we expect the standard deviation of the ratio to be proportional to $\varepsilon|\nabla\tau|$. This standard deviation may increase when $\hat{V}$ is not a smooth function. The resolution of the reconstruction of τ may similarly be estimated from (14): we want $\varepsilon\nabla\tau$ to be small compared to the variations of $\hat{V}_{y_0}(q)$ for q in the vicinity of $|k|\phi$ for otherwise the ratio in (14) is not longer deterministic. Note that the resolution and statistical stability of (14) depend on the statistical structure of the underlying sound speed variations V.

Statistical Stability with more realistic scattering in the one-dimensional case. We conclude this section by revisiting (5) when $V_{y_0}\big((y-y_0)/\varepsilon\big)$ does not have a compact support (i.e. the Fourier transform $\hat{V}(\xi)$ of the random fluctuations is not smooth). This assumption essentially implied above that scattering was only considered in the $\varepsilon-$vicinity of y_0, while scattering farther away from y_0 was assumed to have a marginal effect on the measurements.

We now briefly consider a more realistic scenario for $V_{y_0}(y)$. Since the analysis is significantly more involved, the calculations will be presented in a one-dimensional setting. Consider the one-dimensional model with $x_0 = z_0 = 0$ and $y_0 > 0$ with $t = 2y_0$ then and $k = -|k|$. Then the measurements are of the form

$$v_\varepsilon = \int e^{-\frac{\alpha}{2\varepsilon}x^2} e^{-i\frac{k}{\varepsilon}x} \delta(t-(y-x)-(y-z)) V_{y_0}(\frac{y-y_0}{\varepsilon})(\Delta f)(\frac{z}{\varepsilon}) dy dz dx.$$

This simplifies to

$$v_\varepsilon = \int e^{-\frac{\alpha}{2\varepsilon}x^2} e^{-i\frac{k}{\varepsilon}x} V_{y_0}(\frac{x+z}{2\varepsilon})(\Delta f)(\frac{z}{\varepsilon}) dz dx.$$

We assume $\Delta f \approx \delta$ since integrations in the variable z are easy to deal with when Δf is integrable. Thus we have

$$v_\varepsilon \approx \int e^{-\frac{\alpha}{2\varepsilon}x^2} e^{-i\frac{k}{\varepsilon}x} V_{y_0}(\frac{x}{2\varepsilon}) dx.$$

If $V_{y_0}(x/2\varepsilon)$ is uniformly integrable, then the above is nothing but $\hat{V}_{y_0}(2k)$ in the limit, which leads to the same formula as (13). When $V_{y_0}(x/2\varepsilon)$ is not uniformly integrable, which is the case in practice, then the calculations are much more complicated. The reason $V_{y_0}(x/2\varepsilon)$ cannot be expected to be integrable is that scattering occurs at the scale ε over a domain of size $O(1)$. At the scale ε, the support of V_{y_0} is therefore a domain of size $O(1/\varepsilon)$. Assuming that V is a stationary process, which means that its statistics are independent of spatial translation is a realistic assumption, then we cannot expect $V_{y_0}(x/2\varepsilon)$ to be integrable on its support independently of ε.

Note that with τ present we have to analyze

$$v_{\varepsilon\tau} \approx \int e^{-\frac{\alpha}{2\varepsilon}x^2} e^{-i\frac{k}{\varepsilon}x} V_{y_0}(\frac{x}{2\varepsilon} + \tau(y_0+x)) dx. \tag{15}$$

After rescaling this is, up to a multiplicative constant

$$\int e^{-\frac{\varepsilon\alpha}{2}x^2}e^{-ikx}V_{y_0}(\frac{x}{2}+\tau(y_0+\varepsilon x))dx=\int e^{-\frac{\varepsilon\alpha}{2}x^2}e^{-ikx}e^{iq(\frac{x}{2}+\tau(y_0+\varepsilon x))}\hat{V}_{y_0}(q)dqdx. \tag{16}$$

Let us replace $\tau(y_0+\varepsilon x)$ by $\tau(y_0)+\varepsilon x\tau'(y_0)$ up to a lower-order term that we assume is negligible. Let us also assume that $V_{y_0}(x)$ is a superposition of plane waves

$$V_{y_0}(x)=\sum_j V_j e^{-iq_j x},$$

with V_j random variables and increasing q_j, for instance $q_j=jq$ for a fixed q and $j\in\mathbb{Z}$. This would correspond to a 2π-periodic function, which forms a reasonable approximation for a random medium. For such a model we find that the ratio of integrals of interest is

$$\frac{v_{\varepsilon\tau}}{v_\varepsilon}\approx\frac{\sum_j V_j e^{iq_j\tau(y_0)}e^{-\frac{1}{2\varepsilon\alpha}\left(q_j(\frac{1}{2}+\varepsilon\tau'(y_0))-k\right)^2}}{\sum_j V_j e^{-\frac{1}{2\varepsilon\alpha}\left(q_j\frac{1}{2}-k\right)^2}}.$$

In the analysis of such a ratio, the choice of k and α is more important than in the preceding sections. We need as before $\varepsilon\alpha$ to be small in order to obtain some accuracy in frequency. Then, in order to receive some signal at the detector array, we need $\frac{1}{2}q_j-k$ to be small for one j. Let us assume that there is a $j=j_0$ such that $\frac{1}{2}q_j-k$ is small. This means that k cannot be chosen entirely arbitrary. Let us then assume that $\varepsilon\alpha$ is of the same order as (or smaller than) $(\frac{1}{2}q_j-k)^2$. This shows that only one exponential term above is not negligible and we obtain the approximation for the ratio

$$\frac{v_{\varepsilon\tau}}{v_\varepsilon}\approx\frac{e^{iq_j\tau(y_0)}e^{-\frac{1}{2\varepsilon\alpha}\left(q_j(\frac{1}{2}+\varepsilon\tau'(y_0))-k\right)^2}}{e^{-\frac{1}{2\varepsilon\alpha}\left(q_j(\frac{1}{2}-k)\right)^2}}\approx e^{2ik\tau(y_0)}\,(1+O(\sqrt{\varepsilon\alpha}))\,e^{-\frac{\frac{1}{2}q_j-k}{\sqrt{\varepsilon\alpha}}\frac{\varepsilon\tau'(y_0)q_j}{\sqrt{\varepsilon\alpha}}}.$$

The latter term is close to 1 if $\varepsilon\tau'(y_0)\ll\sqrt{\varepsilon\alpha}$. When this is the case, we obtain that the ratio is given by

$$e^{i2k\tau(y_0)}\left(1+O(\sqrt{\varepsilon\alpha})+O(\frac{\varepsilon|\tau'(y_0)|}{\sqrt{\varepsilon\alpha}})\right).$$

We thus observe that if α is chosen on the order of $|\tau'(y_0)|$, then the ratio provides the correct phase shift $e^{i2k\tau(y_0)}$ up to an error that is small provided that $\varepsilon|\tau'|\ll 1$.

The conclusions are therefore the same as those obtained before: the displacement is accurately reconstructed provided that $\varepsilon\|\tau'\|_\infty\ll 1$. This shows that the best resolution we expect from the method is much larger than ε. Note also that the conclusion now holds provided that k and α are carefully chosen. Note finally that the ratio of interest is close to being of unit modulus for the appropriate choices of (α,k).

Generalization to three dimensions. The generalization to the three dimensional setting of the above calculations is more difficult and will not be presented here in detail. What we obtain as a generalization of (15) is that

$$v_{\varepsilon\tau} \approx C_\varepsilon \int e^{i\frac{|k|}{\varepsilon}\phi\cdot(y-y_0)} e^{-\frac{\alpha}{2\varepsilon}(\phi\cdot(y-y_0))^2} e^{-\frac{|k|^2}{2\varepsilon\alpha}\left(\left|(I-\hat{k}\otimes\hat{k})\frac{(y-y_0)}{|y_0-x_0|}\right|^2\right)} V\big(\frac{y}{\varepsilon}+\tau(y_0+y)\big)dy.$$

We now observe two length scales in the above quadratic exponentials above: $(\frac{|k|^2}{\varepsilon\alpha})^{-\frac{1}{2}}$ and $(\frac{\alpha}{\varepsilon})^{-\frac{1}{2}}$, with the above approximation involving errors proportional to these two scales. From this, we infer that $v_{\varepsilon\tau}/v_\varepsilon$ is close to $e^{i|k|\phi\cdot\tau(y_0)}$ provided that τ is sufficiently constant in the vicinity of y_0 for these two scales. This implies that the ratio $v_{\varepsilon\tau}/v_\varepsilon$ is

$$e^{i|k|\phi\cdot\tau(y_0)}\Big(1+O\Big(\big(\frac{\sqrt{\varepsilon}}{\sqrt{\alpha}}+\frac{\sqrt{\varepsilon\alpha}}{|k|}\big)\big(1+|\nabla\tau(y_0)|\big)\Big)\Big).$$

The term in $\frac{\sqrt{\varepsilon}}{\sqrt{\alpha}}|\nabla\tau(y_0)|$ is similar to that in the one-dimensional setting. The following term in $\frac{\sqrt{\varepsilon\alpha}}{|k|}|\nabla\tau(y_0)|$ comes from the multi-dimensional angular spreading. We observe that the optimal choice for α is $|k|$ as indicated earlier, which corresponds to both a good range resolution (the term $\frac{\sqrt{\varepsilon}}{\sqrt{\alpha}}$) as well as good cross-range resolution (the term $\frac{\sqrt{\varepsilon\alpha}}{|k|}$). With proper dimensional quantities, the above result yields (5).

4 Numerical simulations

In this section, we illustrate our reconstruction procedure by numerical simulations in a two-dimensional setting. Instead of solving a homogeneous initial value problem, the incident field is solution of the inhomogeneous problem (again up to a scaling factor)

$$(\partial_t^2-\Delta)u_0 = h\left(\frac{t}{\varepsilon}\right)\, g_0\left(\frac{|x-z_0|}{\varepsilon^p}\right),$$

completed with zero initial condition. Where $h(t)$ is a C^∞ bump function of support $[-1/2,1/2]$ defined by $h(t)=e^{\frac{1}{4t^2-1}}$ inside its support and the function g_0 have a bounded support around the origin, is positive and unitary in the L^1 norm.

We present two different configurations described figure 2. In both configurations we assume that V is made of N_ε localized heterogeneities of random positions and amplitudes:

$$V(y) = \sum_{i=1}^{N_\varepsilon} \rho_i(\omega)\, g_i\left(\frac{y_i^\varepsilon(\omega)-y}{\varepsilon^p}\right).$$

This specific form of random field is described in [24] (chap. 8.2, eq. (8.51)). The amplitudes $\rho_i \in [-1,1]$ are independent uniformly distributed random variables, whereas the $\{y_i^\varepsilon(\omega)\}$ are distributed randomly inside a rectangle for the first configuration and along a line for the second. Every scatterer, as well as z_0, are contained in the plane $x\cdot e_3=0$. Therefore, the scattered field is symmetric with respect to this plane and its contribution outside the plane can be omitted in formula (1).

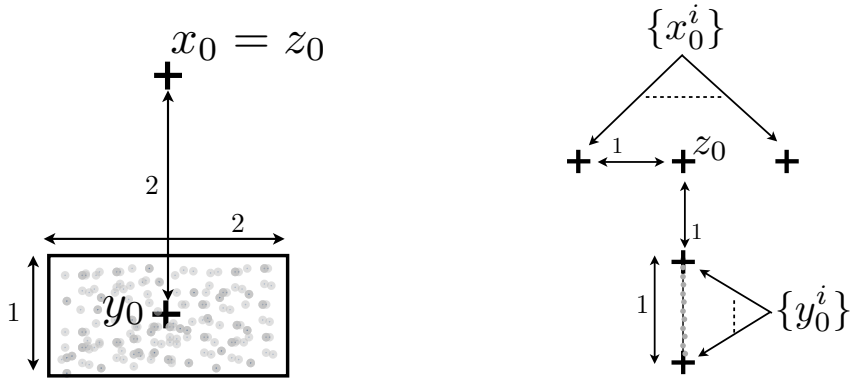

(a) Scatterers randomly distributed in a rectangle

(b) Scatterers randomly distributed along a line

Figure 2: Schematic of the two configurations presented, where (x_0, z_0) respectively are the source and observation positions and y_0 the position where the displacement τ is recovered.

Explicit form of the scattered field. Assuming p large enough we approximate V and the source term using point scatterers approximation. Instead of (9) the scattered field is given by

$$u_\tau(t,x) \equiv \sum_{i=1}^{N_\varepsilon} \rho_i(\omega)\, \frac{h\left(\varepsilon^{-1}\left(t - |x - y_i^\varepsilon - \varepsilon\,\tau(y_i^\varepsilon)| - |z_0 - y_i^\varepsilon - \varepsilon\,\tau(y_i^\varepsilon)|\right)\right)}{|x - y_i^\varepsilon - \varepsilon\tau(y_i^\varepsilon)|\,|x_0 - y_i^\varepsilon - \varepsilon\tau(y_i^\varepsilon)|}. \tag{17}$$

Computation of the FBI transform. The windowed Fourier transform $v_\tau(t_0, x_0, k)$ given by (1) of $u_\tau(t,x)$ given by (17) are computed at the observation locations in the plane $x \cdot e_3 = 0$, i.e we restrict the computation of the FBI to a quadrature in that plane. The quadrature is a composite 3-point Gauss quadrature formula on a cartesian squared grid centered at x_0. The size d_ε and the spacing dr_ε of the grid are

$$d_\varepsilon^2 = 4\,\varepsilon\,\ln\left(2\,\varepsilon^{-\frac{1}{2}}\right), \quad dr_\varepsilon = \frac{\varepsilon}{3\,k}. \tag{18}$$

The choice of d_ε as given by (18) guarantees that the error made by restricting the integral into a bounded domain is of order $\varepsilon^{\frac{1}{2}}$.

Configuration a). We choose $x_0 = z_0 = (0,0,0)$, $\alpha = 1$, $|k| = 1$, $\varepsilon = 5 \times 10^{-4}$, $N_\varepsilon = 10^6$. The scatterers are such that $\{y_i^\varepsilon(\omega)\} \subset D$ with $D = [-1,1] \times [-5/2, -3/2]$ and are uniformly distributed in a squared subdomain of D of area $1/N_\varepsilon$, the unions of these subdomains being D. We choose t_0 such that $y_0 = (0,-2,0)$.

Configuration b). We assume that the distribution of scatterers is contain in D along a finite straight line (see Figure 2):

$$L = \left\{(0,l,0) \in \mathbb{R}^3, \quad l \in [-2,-1]\right\}.$$

The points $\{y_i^\varepsilon(\omega)\}$ are then distributed randomly via the formula

$$y_i^\varepsilon(\omega) = \left(0,\, -1 - \frac{i-1}{N_\varepsilon} - \frac{\hat{y}_i(\omega)}{N_\varepsilon},\, 0\right)$$

where $\hat{y}_i(\omega) \in [0,1]$ is uniformly distributed and $N_\varepsilon = 10^4$. The source term is located at $z_0 = (0,0,0)$, $|k| = 1$ and $\varepsilon = 5 \times 10^{-4}$.

A priori reconstruction quality informations (configuration a). We arbitrarily choose

$$\tau(y) = \frac{1}{100}\big(\cos(\pi\, y_1),\, 2\,\cos(\pi\, y_1),\, 0\big).$$

Figure 3 represents the reconstruction of $\tau(y_0)\cdot\phi$ for different random realization of V_{y_0} which is numerically given by the formula

$$\tau(y_0)\cdot\phi = \frac{1}{|k|}\arg\left(\frac{v_{\varepsilon\tau}(|x_0-y_0|+|y_0-z_0|,x_0,k)}{v_\varepsilon(|x_0-y_0|+|y_0-z_0|,x_0,k)}\right). \tag{19}$$

Since $\phi = (0,2,0)$ we have $\tau(y_0)\cdot\phi = 4/100$. The average over the discrete reconstruction is 0.398 which is close to what is expected. However we observe in Figure 3 the correlation between the quality of the reconstruction and

- the amplitude of $|v_\varepsilon|$: if almost no energy is measured in the configuration at rest, then we cannot expect a good reconstruction.
- the deviation of $|v_{\varepsilon\tau}/v_\varepsilon|$ from unity: our asymptotic analysis predicted this ratio to be of module approximately equal to 1 (see equation (3)).

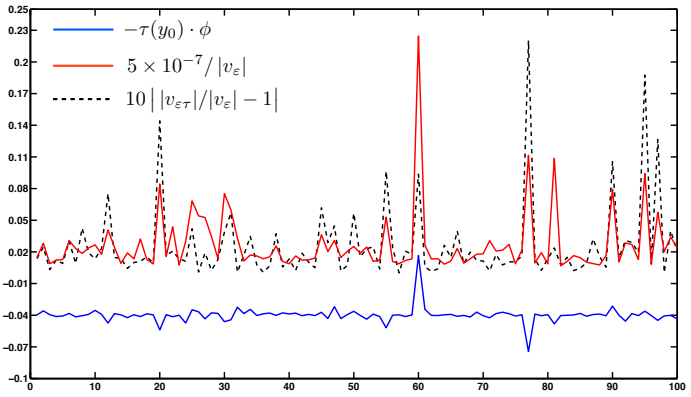

Figure 3: For different random realizations of V: reconstructed $\tau(y_0)\cdot\phi$ (the average value is approximately 0.398), amplitude of the measurement without shift and deviation of the ratio $|v_{\varepsilon\tau}/v_\varepsilon|$ with respect to 1.

Full reconstruction with minimal informations (configuration b). We now arbitrarily use the following 2D vector fields to model the displacement

$$\tau(y) = \frac{5}{100}\big(\sin(10\,\pi\, y_2),\, \frac{1}{2}\cos(8\,\pi\, y_2),\, 0\big). \tag{20}$$

We first compute the windowed Fourier transforms at the observation points $x_0 = (-1, 0, 0)^T$ and $\tilde{x}_0 = (1, 0, 0)^T$ at well chosen time such that the set of reconstruction point $\{y_0^i\}$ is uniformly distributed along L. Since we recover $\tau(y_0) \cdot \phi$ and $\tau(y_0) \cdot \tilde{\phi}$ with $(\phi, \tilde{\phi})$ a basis of $\mathbb{R}^2$ we can recover $\tau(y)$ completely. Figure 4 shows the two components of the reconstructed displacement τ function on 100 sampling points distributed uniformly along L for a single realizations of V.

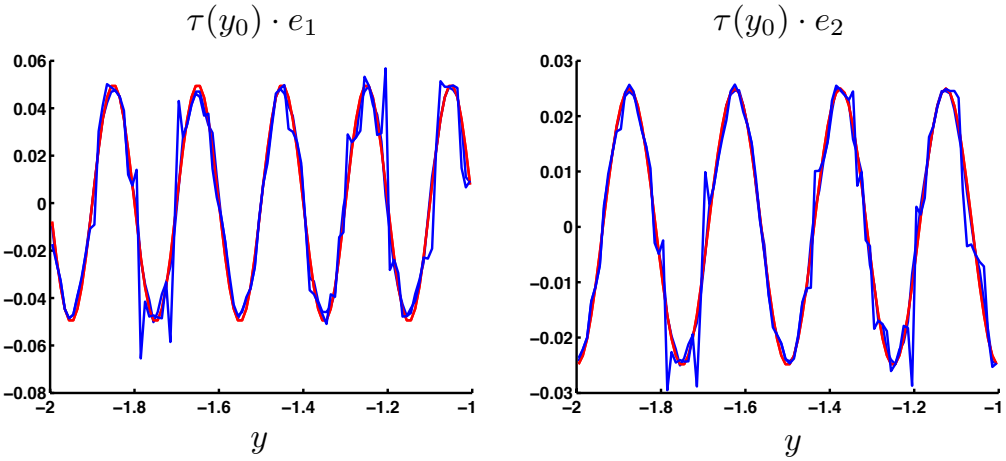

Figure 4: Reconstructed displacement in both directions compared to the exact oscillating displacement given by (20).

Improved reconstruction at several observation positions (configuration b). Following our theoretical analyses, we suggest a variant of the algorithm presented above. We now assume that the FBI transforms are computed at a every point x_0^i of a set of N observations points $\{x_0^i\}$. For each triplet (x_0^i, y_0^j, z_0) we define the vector ϕ_j^i using equations (3, 4). Applying formula (19) the quantity $\tau(y) \cdot \phi_j^i$ can be recovered at every y_0^j. This means that the reconstruction of the full vector field $\tau(y)$ is redundant as soon as N is large enough. An alternative to standard least-square fitting is to select among our measurements, a couple $(\{v_{\varepsilon,j}^{n_j}, v_{\tau\varepsilon,j}^{n_j}\}, \{v_{\varepsilon,j}^{m_j}, v_{\tau\varepsilon,j}^{m_j}\})$, for 2D reconstruction or a triplet, for 3D reconstruction, that are likely to give more stable results. To do so we choose the scattered fields that have the strongest amplitude, more precisely, we define

$$v_{\varepsilon,j}^i = v_\varepsilon(|x_0^i - y_0^j| + |y_0^j - z_0|, x_0^i, k),$$

and assume that for all j fixed the $\{\phi_j^i\}$ are 2-by-2 independent (any combination of them give access to the full field $\tau(y)$ since we reconstruct 2D displacement). The selected measurements correspond to the couple of indices (n_j, m_j) such that

$$|v_{\varepsilon,j}^{n_j}| \geq |v_{\varepsilon,j}^{m_j}| \geq |v_{\varepsilon,j}^i|, \quad \forall i \notin \{n_j, m_j\}.$$

The displacement τ can be recovered at each y_0^j since

$$\frac{v_{\tau\varepsilon,j}^{n_j}}{v_{\varepsilon,j}^{n_j}} \simeq e^{i|k|\tau(y_0^j)\cdot\phi_j^{n_j}} \qquad \frac{v_{\tau\varepsilon,j}^{m_j}}{v_{\varepsilon,j}^{m_j}} \simeq e^{i|k|\tau(y_0^j)\cdot\phi_j^{m_j}},$$

and the vectors $\phi_j^{n_j}$ are $\phi_j^{m_j}$ independent by assumption. Figure 5 shows the results obtained using such algorithm when the $\{x_0^i\}$ are uniformly distributed along a line:

$$x_0^i = \big(0,\, -1 + \frac{2(i-1)}{N-1},\, 0\big), \quad N = 30$$

Results given figure 5 show the efficiency of such approach: the reconstruction is more stable statistically.

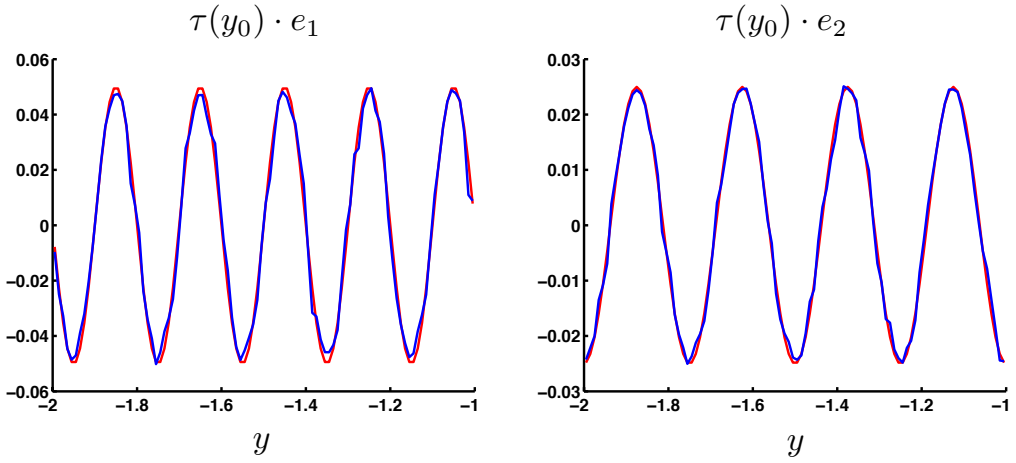

Figure 5: Improved reconstructed displacement in both directions compared to the exact oscillating displacement given by (20).

Improved reconstruction at several frequencies (configuration b). The previous algorithm required the measurements of the scattered field at many observation points, which may not be available in practical experiments. In this set up we consider only two observation points $\{x_0^i\} = \{x_0^0, x_0^1\}$ with

$$x_0^0 = (-1, 0, 0), \quad x_0^1 = (1, 0, 0).$$

For the reconstruction we consider a single realization of the random medium and the averaging formula

$$\int \frac{1}{|k+q|} \arg\left(\frac{(w_\tau)(t_0, x_0, k+q)}{w(t_0, x_0, k+q)}\right) d\mu(q),$$

with $|k| = 1$ and $q \in [-1/2, 1/2]$. The other parameters are kept unchanged (except that we choose $dr_\varepsilon = 2\varepsilon/3k$ to take into account the increase of the frequency in the measurements). In Figure 6 we plot the reconstructed displacement for 100 different values of q and in Figure 7 the average reconstructed displacement ($\mu(q)$ is the uniform discrete measure over 100 points uniformly distributed in $[-1/2, 1/2]$). Note that the different reconstruction corresponds only to different post-processing operations of the signal.

We could also obviously combine the two modifications presented above by averaging only on a reduced number of reconstructed displacement corresponding (in each points) to the truncated FBI with the largest amplitude (as described above). The results we obtain in our specific case are

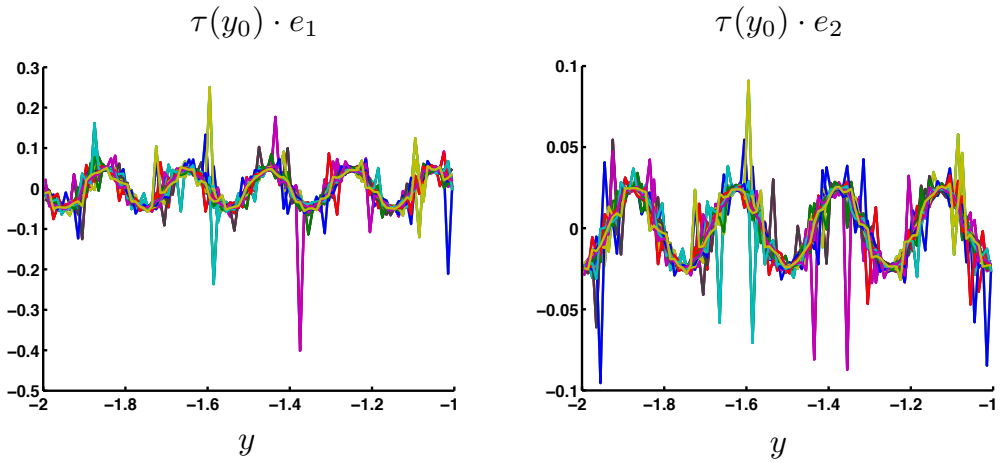

Figure 6: Reconstructed displacement in both directions for different value of $k \in [1/2, 3/2]$.

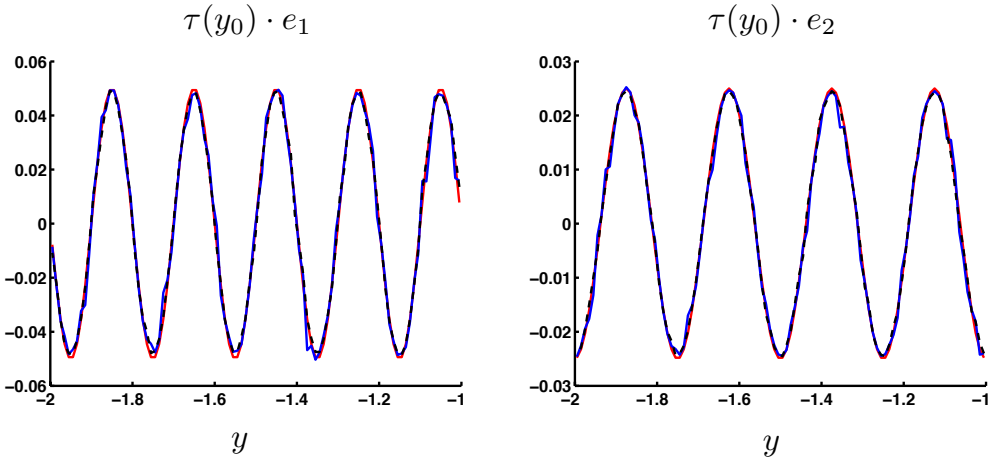

Figure 7: Plain line: reconstructed displacement compared to the exact oscillating displacement given by (20) after averaging all the reconstructions represented Figure 6. Dashed line: reconstructed displacement using the reconstructions represented Figure 6 and the selection algorithm described in the previous paragraph.

slightly improved (see Figure 7 dashed line).

Numerical assessment of formula (14) (configuration b). We now assess the quality of formula (14) with the following set of numerical experiments. We consider only one triplet (x_0, y_0, z_0) with $x_0 = z_0 = (0, 0, 0)$ and $y_0 = (0, -1.5, 0)$ as well as a displacement $\tau(l\,; y)$ parametrized by l:

$$\tau(l\,; y) = \frac{1}{10}\big(0, \arctan(l\, y_2 + l\, 1.5), 0\big) \quad \Rightarrow \quad |\nabla\tau(l\,; -1.5)| = l.$$

For a unique realization of the random medium V_{y_0} we plot in Figure 8 the expression $|v_{\tau(l)\varepsilon}/v_\varepsilon| - 1$ with respect to l for different values of $|k| \in [1/2, 3/2]$. Analysis of Figure 8 shows that

- the numerical results are in agreement with (14): the standard deviation of the ratio is propor-

tional to $|\nabla\tau(l)|$.

- some values of $|k|$ give more stable ratios with respect to the gradient variation, confirming the importance of choosing appropriately k.

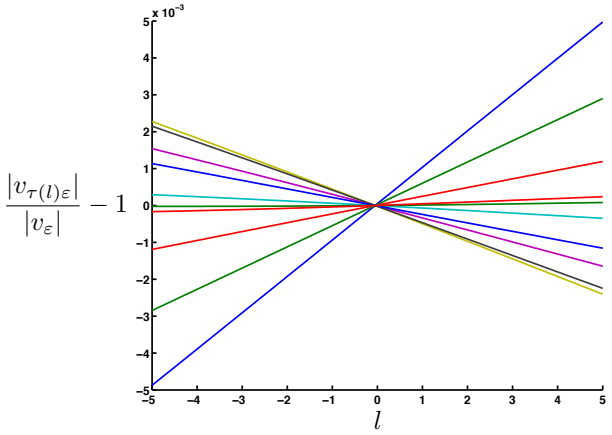

Figure 8: Deviation of the ratio $|v_{\tau(l)\varepsilon}/v_\varepsilon|$ with respect to the gradient of the displacement to be reconstructed for different values of $|k| \in [1/2, 3/2]$.

5 Conclusions

In this paper, we have presented a modeling of the influence of elastic displacements on ultrasound measurements. We have then used this model to propose a vectorial reconstruction of such internal elastic displacements. Our algorithm was justified theoretically and illustrated by several reasonably realistic numerical simulations. Such an algorithm is expected to provide statistically robust reconstructions in elastography, a medical imaging modality aiming to reconstruct the elastic properties of tissues.

The main advantage of the procedure is the simple formula obtained in (4)-(5). It is based on the major assumption that the displacement $\tau(x)$ varies slowly compared to the probing ultrasound pulse. This limits the spatial resolution one expects from such a method. Nonetheless, our theoretical and numerical analyses show that the reconstruction procedure is stable with respect to the randomness in the scattering medium and should provide accurate spatially varying and vectorial reconstructions of elastic displacements in elastography.

Acknowledgment

This research was partially funded by AFOSR Grant NSSEFF- FA9550-10-1-0194 and NSF grant DMS-1108608.

References

[1] G. Bal, *Kinetics of scalar wave fields in random media*, Wave Motion, 43(2) (2005), pp. 132–157.

[2] ——, *Hybrid inverse problems and internal functionals*, Inside Out II, MSRI Publications, G. Uhlmann Editor, Cambridge University Press, Cambridge, UK, 2012.

[3] ——, *Hybrid Inverse Problems and Systems of Partial Differential Equations*, Contemporary Mathematics 615, P. Stefanov, A. Vasy and M. Zworski Editors, A.M.S., USA, 2014.

[4] G. Bal, C. Bellis, S. Imperiale, and F. Monard, *Reconstruction of constitutive parameters in isotropic linear elasticity from noisy full-field measurements*, Accepted; Inverse problems, (2014).

[5] G. Bal and G. Uhlmann, *Reconstruction of coefficients in scalar second-order elliptic equations from knowledge of their solutions*, Comm. Pure Appl. Math., 66 (2013), pp. 1629–1652.

[6] G. Bal and R. Verástegui, *Time Reversal in Changing Environment*, Multiscale Model. Simul., 2(4) (2004), pp. 639–661.

[7] P. E. Barbone, C. E. Rivas, I. Harari, U. Albocher, A. A. Oberai, and Y. Zhang, *Adjoint-weighted variational formulation for the direct solution of inverse problems of general linear elasticity with full interior data*, Int. J. Numer. Meth. Engng, 81 (2010), pp. 1713–1736.

[8] J. Bercoff, M. Tanter, and M. Fink, *Supersonic shear imaging: a new technique for soft tissue elasticity mapping*, IEEE Trans. Ultrason. Ferroelectr. Freq. Control, 51 (2004), pp. 396–409.

[9] J.-L. Gennisson, T. Deffieux, M. Fink, M. Tanter,, *Ultrasound elastography: Principles and techniques*, Diagnostic and Interventional Imaging, 94 (2013), pp. 487–495.

[10] S. Chandrasekhar, *Radiative Transfer*, Dover Publications, New York, 1960.

[11] L. Evans, *Partial Differential Equations*, Graduate Studies in Mathematics Vol.19, AMS, 1998.

[12] P. Kuchment and D. Steinhauer, *Stabilizing inverse problems by internal data*, Inverse Problems, 28 (2012), 084007.

[13] P.-D. Létourneau and G. Bal, *Resolution and de-aliasing in Ultrasound Elastography*, submitted, 2015.

[14] K. Lin and J. R. McLaughlin, *An error estimate on the direct inversion model in shear stiffness imaging*, Inverse Problems, 25 (2009), 075003.

[15] J. R. McLaughlin, N. Zhang, and A. Manduca, *Calculating tissue shear modulus and pressure by 2D log-elastographic methods*, Inverse Problems, 26 (2010), 085007.

[16] R. Muthupillai, D. J. Lomas, P. J. Rossman, J. F. Greenleaf, A. Manduca, and R. L. Ehman, *Magnetic resonance elastography by direct visualization of propagating acoustic strain waves*, Science, 269 (1995), pp. 1854–1857.

[17] G. Nakamura, Y. Jiang, S. Nagayasu, and C. Jin, *Inversion analysis for magnetic resonance elastography*, Appl. Anal., (2008), p. 165179.

[18] J. Ophir, I. Céspedes, H. Ponnekanti, Y. Yazdi, and X. Li, *Elastography: A quantitative method for imaging the elasticity of biological tissues*, Ultrasonic Imaging, 13 (1991), pp. 111–134.

[19] J. Ophir et al., *Elastography: Imaging the elastic properties of soft tissues with ultrasound*, J. Med. Ultrasonics, 29 (2002), pp. 155–171.

[20] M. M. Doyley, *Model-based elastography: a survey of approaches to the inverse elasticity problem*, Physics in Medicine and Biology, 57 , (2012), pp. 35–73.

[21] K. J. Parker, M. M. Doyley, and D. J. Rubens, *Imaging the elastic properties of tissues: the 20 year perspective*, Phys. Med. Biol., 56 (2011), pp. R1–R29.

[22] L. Ryzhik, G. C. Papanicolaou, and J. B. Keller, *Transport equations for elastic and other waves in random media*, Wave Motion, 24(4) (1996), pp. 327–370.

[23] R. Zahiri-Azar and S. E. Salcudean, *Motion estimation in ultrasound images using time domain cross correlation with prior estimates*, IEEE, Transactions on Biomedical engineering, 53(10) (2006), pp. 1990–2000.

[24] S. Torquato, *Random heterogeneous materials*, Interdisciplinary Applied Mathematics, Springer-Verlag, New York, 16 (2002).